The Influence of Plasma-Based Nitriding and Oxidizing Treatments on the Mechanical and Corrosion Properties of CoCrMo Biomedical Alloy

FOTINI NOLI, LUC PICHON, and ORHAN ÖZTÜRK

Plasma-based nitriding and/or oxidizing treatments were applied to CoCrMo alloy to improve its surface mechanical properties and corrosion resistance for biomedical applications. Three treatments were performed. A set of CoCrMo samples has been subjected to nitriding at moderate temperatures (~ 400 °C). A second set of CoCrMo samples was oxidized at 395 °C in pure O_2. The last set of CoCrMo samples was nitrided and subsequently oxidized under the experimental conditions of previous sets (double treatment). The microstructure and morphology of the layers formed on the CoCrMo alloy were investigated by X-ray diffraction, Atomic Force Microscopy, and Scanning Electron Microscopy. In addition, nitrogen and oxygen profiles were determined by Glow Discharge Optical Emission Spectroscopy, Rutherford Backscattering Spectroscopy, Energy-Dispersive X-ray, and Nuclear Reaction Analysis. Significant improvement of the Vickers hardness of the CoCrMo samples after plasma nitriding was observed due to the supersaturated nitrogen solution and the formation of an expanded FCC γ_N phase and CrN precipitates. In the case of the oxidized samples, Vickers hardness improvement was minimal. The corrosion behavior of the samples was investigated in simulated body fluid (0.9 pct NaCl solution at 37 °C) using electrochemical techniques (potentiodynamic polarization and cyclic voltammetry). The concentration of metal ions released from the CoCrMo surfaces was determined by Instrumental Neutron Activation Analysis. The experimental results clearly indicate that the CoCrMo surface subjected to the double surface treatment consisting in plasma nitriding and plasma oxidizing exhibited lower deterioration and better resistance to corrosion compared to the nitrided, oxidized, and untreated samples. This enhancement is believed to be due to the formation of a thicker and more stable layer.

https://doi.org/10.1007/s11661-018-4487-5

I. INTRODUCTION

CoCrMo alloy (ISO 5832-12) is known as a metallic biomaterial. Its mechanical properties and corrosion resistance render it one of the dominant alloys for total joint arthroplasty.[1–3] Since hundreds of thousands of patients around the world have used implant materials for years, the quality and lifetime of the implants as well as the biological effects are of great concern. The requirements of the prosthesis materials such as high wear resistance, excellent corrosion properties, and biocompatibility are generally fulfilled using conventional biomaterial. However, there is a general recognition that the long-term total joint replacement may be associated with metal-degradation products. Biological reactions induced by corrosion and wear products of the implants are still a major focus in biomedical material research.[4,5] Biomaterials fabricated from CoCr-based alloys are reported to release increased concentrations of Co, Cr, and Ni ions in simulated body fluids.[6–8] Therefore, efforts have mainly focused on the modification of the surfaces of the implants to improve their mechanical properties, specifically lifetime.

Nitrogen implantation is one of many surface treatment techniques forming protective layers on Fe- and Co-based alloys and inducing enhanced surface properties, especially improved mechanical properties, without affecting the bulk.[5,9,10] Plasma-assisted nitriding[6,11–19] and plasma-based ion implantation (PBII)[15,19–21] are found to improve considerably the mechanical properties of CoCr alloys (*e.g.*, wear and fatigue resistance) producing thick modified surface layers. Furthermore, both surface treatment techniques can be achieved on

FOTINI NOLI is with the Department of Chemistry, Aristotle University, 54124, Thessaloniki, Greece, Contact e-mail: noli@chem.auth.gr LUC PICHON is with the Institut Pprime - UPR 3346 CNRS, Université de Poitiers, ISAE-ENSMA, 86962, Poitiers, France. ORHAN ÖZTÜRK is with the Department of Physics, Izmir Institute of Technology, Gulbahce-Urla, 35430, Izmir, Turkey.

Manuscript submitted May 17, 2017.
Article published online February 5, 2018

complex shape parts and significantly improve the tribological and corrosion properties of the treated surfaces.[22,23]

At moderate nitriding temperatures (typically below 400 °C), nitrogen is incorporated in solid solution in the initial FCC γ phase. This leads to the so-called metastable expanded FCC γ_N phase, also called S-phase, which is characterized by high in-plane residual compressive stresses.[11,24] With increasing temperature and treatment duration, the γ_N phase is partially decomposed into nitride precipitates (CrN, Cr_2N) and residual γ phase with lower Cr content.[12,13,16]

Although nitriding treatment has been observed to have beneficial effect on the mechanical properties of CoCrMo, its influence on the corrosion behavior is still under investigation. Nitriding treatments are usually observed to be detrimental to the corrosion resistance.[23] Chromium atoms, more or less bonded to nitrogen, are no longer mobile to create the protective passive oxide layer and cobalt has a weakened chemical bond. In comparison to the untreated CoCrMo alloy, higher cobalt ions are released from surface during corrosion. Moreover, this release is found to be enhanced by the rougher nature of the nitrided surface.[5,21]

The nitrided layer usually presents superior wear resistance under dry conditions due to its higher hardness.[13,14,21,25–28] However, the tribocorrosion behavior is much more complex as the nitrided CoCr alloys behavior is highly dependant on the corrosion medium, on the applied potential, on the counterpart materials (CoCrMo, UHWMPE, WC, Al_2O_3), and on the wear conditions (sliding, fretting, applied load, revolution speed, and frequency). Tribological tests in simulated body fluid (SBF) or bovine serum on nitrided CoCr alloys often lead to significant decrease of the wear volume although the wear is clearly enhanced by the corrosion process.[14,21] Ortega-Saenz et al. observed diminished corrosion and wear resistance in Ringer's solution of CoCrMo nitrided at 520 °C.[29] Bazzoni *et al.* have recently shown that the wear in a 0.9 pct NaCl solution of untreated or nitrided CoCrMo at 350 °C, depends on the applied potential: the formed γ_N phase is no more passive and enables a constant and limited wear rate on a wide range of potential. On the contrary, the tribocorrosion of the untreated CoCrMo becomes catastrophic at high anodic potential.[6] Lutz et al. noticed that nitriding at moderate temperature (below 400 °C) induces a limited increase of metal ions release but on the other hand reduction of the wear debris particles was observed.[21] Guo *et al.* reported that N-implantation into CoCrMo induces a novel composite microstructure of the nanocrystalline CrN which enhances hardness, corrosion, and tribocorrosion properties and Ba et al. found that plasma nitriding produces thicker, harder, and higher wear-resistant layers than the conventional CoCrMo alloys.[30,31] Therefore, nitriding can be beneficial in prosthesis applications depending on the combination of wear and corrosion processes induced by the chemical and tribological solicitations.

In this work, a double surface treatment at moderate temperatures (around 400 °C) of CoCrMo alloy was performed that consisted in a plasma-assisted nitriding and a subsequent plasma-assisted oxidation. Influence of the double treatment on the mechanical and corrosion properties of the CoCrMo sample is investigated and compared to the nitrided, oxidized, and untreated samples. Indeed, oxygen implantation in CoCrMo, coupled with or without a prior nitrogen implantation, was shown to improve the wear resistance in dry conditions or Hank's solution and moreover to reduce the metal ions release.[10,32–34] Surface characterization techniques were applied before as well as after the corrosion tests in simulated body fluid (0.9 pct NaCl at 37 °C) to obtain information concerning the long-term stability of the modified materials under selective experimental conditions. Since the effects of metal ions released from the biomaterials is of great concern, the concentration of the metals in the solution after the electrochemical tests was determined by Neutron Activation Analysis (NAA). As a complement to a previous short communication,[35] which had mainly focused on the characterizations of the samples by accelerator-based ion-beam techniques, this article is devoted to provide results in much more detail and complementary discussion. The SEM, AFM, XRD, and GDOES characterizations of treated samples before and after corrosion tests are thoroughly described to understand the influence of the surface treatment on the corrosion behavior.

II. EXPERIMENTAL

A. *Sample Preparation*

A medical grade CoCrMo alloy (ISO 5832-12) with grain size ranging from 5 to 15 μm was used as substrate (composition Cr:27.66, Mo:5.60, Al:0.01, Ti:0.01, C:0.048, Zr:0.01, Fe:0.08, and Co:~ 65 all in wt pct). Flat disks of 15 mm diameter and thickness of 3 mm were polished with increasing grade SiC papers. Polishing was then completed using diamond suspension (6 to 0.25 μm) and finally a colloidal suspension of alumina (0.01 μm).

Three sets of samples were prepared using nitrogen and/or oxygen plasma at moderate temperature. The first set of samples (denoted CoCrMo + N) was plasma nitrided at 400 °C in 60 mTorr (8 Pa) of N_2–H_2 (60 to 40 vol pct for a total introduced flow of 100 sccm), with R.F. plasma excitation of 700 W (13.56 MHz), for 150 minutes. The second set (denoted CoCrMo + O) was plasma oxidized at 400 °C in 60 mTorr (8 Pa) of pure O_2 (40 sccm) with R.F. plasma excitation of 700 W for 120 minutes. The double treatment consisting in plasma nitriding and subsequent oxidizing was applied to the CoCrMo samples of the third set (denoted CoCrMo + N + O) under the experimental conditions of previous sets. More details about the experimental set-up are given elsewhere.[36] Before any investigation, the samples were cleaned after rinsing in deionized water and alcohol.

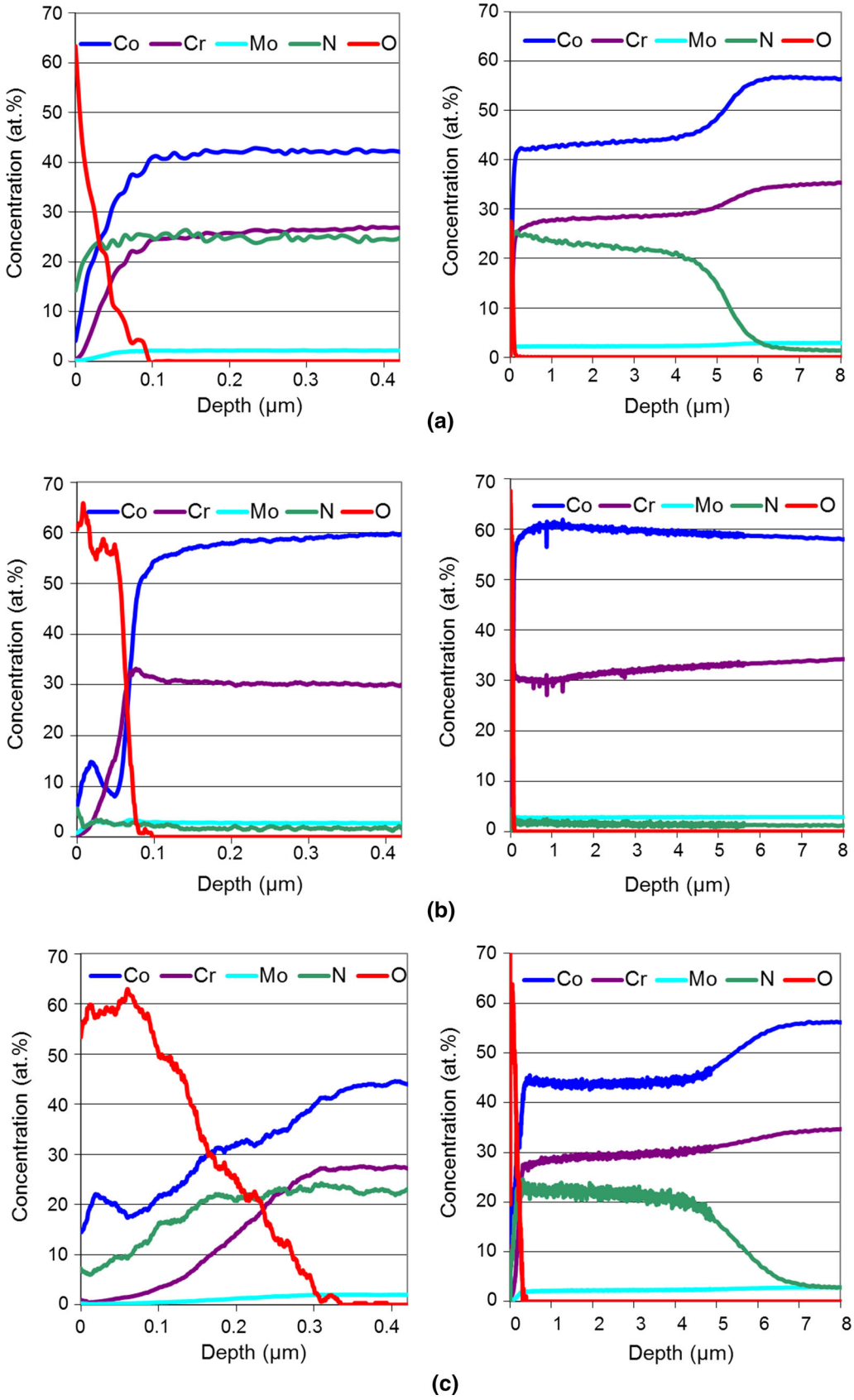

Fig. 1—Elemental profiles in at. pct from GDOES measurements at the surface of (*a*) nitrided CoCrMo sample (CoCrMo + N), (*b*) oxidized CoCrMo sample (CoCrMo + O), and (*c*) double-treated CoCrMo sample (CoCrMo + N + O); (profiles on the left are enlarged views of the overall profiles on the right).

B. *Sample Characterization*

The phases present on the nitrogen and oxygen plasma-processed surfaces of the CoCrMo samples were determined by X-ray diffraction (XRD) using a Philips X'pert diffractometer with Cu-Kα radiation (λ = 1.54 Å) in Bragg-Brentano ($\theta/2\theta$) and grazing incidence (GIXRD) geometries ($\omega/2\theta$). The latter geometry is primarily used for probing thin oxide layers since at grazing incidence angles the penetration of X-rays into a surface is reduced. GIXRD was carried out at grazing angles of ω = 1 and 3 deg. The probed depth at ω = 1 deg is estimated to be about 100 nm.

The chemical composition and the elemental profiles of the modified layers were investigated by Glow Discharge Optical Emission Spectroscopy (GDOES). Performed on a commercial Jobin-Yvon GD-Profiler^{TM}, the quantification by GDOES has an absolute accuracy better than 1 at. pct for metallic elements and about 3 at. pct for nitrogen and oxygen (depth resolution better than 10 nm nearby the surface).

Rutherford Backscattering Spectroscopy (RBS) and/or Nuclear Reaction Analysis (NRA) using 1.35 MeV deuteron beams (5.5 MeV Tandem Accelerator) were also applied. For the determination of the nitrogen and oxygen content of the samples by NRA, the $^{14}N(d,p)^{15}N$, $^{14}N(d,\alpha)^{12}C$, and $^{16}O(d,p)^{17}O$ nuclear reactions were used.[35]

Structural and topographical changes on the surfaces of plasma nitrided, oxidized, and double-treated CoCrMo samples were studied by Scanning Electron Microscopy (SEM) (Philips XL-305 FEG). Supplemental data related to nitrogen and oxygen contents of the plasma-treated surfaces were obtained by Energy-dispersive X-ray Spectroscopy (EDS).

The SEM/EDS examination of the samples after the corrosion tests was performed using a different SEM system (JEOL JSM 840A electron microscope) equipped with an EDS INCA micro-analytical system. The operating conditions were accelerating voltage 20 kV, probe current 45 nA, and counting time 60 seconds, with ZAF correction being provided on-line.

Atomic force microscopy (AFM) on treated CoCrMo surfaces was applied in tapping mode using the commercial systems, Veeco 4.1 and NT-MDT Solver PRO AFM/STM. The scan area for all the surfaces was 30 × 30μm. An average roughness (Ra) was estimated based on at least three measurements obtained on different regions.

Surface microhardness was determined on a Shimatsu Vickers microhardness tester with loads from 25 to 500 g. The remaining indent depth was calculated by dividing the measured diagonal length of the remaining indentation imprints by 7 (considering the indentor geometry). This remaining penetration depth was found to vary from 1 micron to less than 10 μm, depending on the load and on the microhardness of the sample. The penetration depth is then higher or similar to the thickness of the formed layers. So, the obtained hardness is not representative of the layer itself but includes also a more or less significant influence of the bulk material. All the obtained values are averaged over 5 independent measurements.

C. *Corrosion Tests*

The corrosion behavior was investigated by means of potentiodynamic and cyclovoltammetric techniques according to ASTM Designation G5-82.[37,38] Simulated body fluid conditions were applied using a solution of

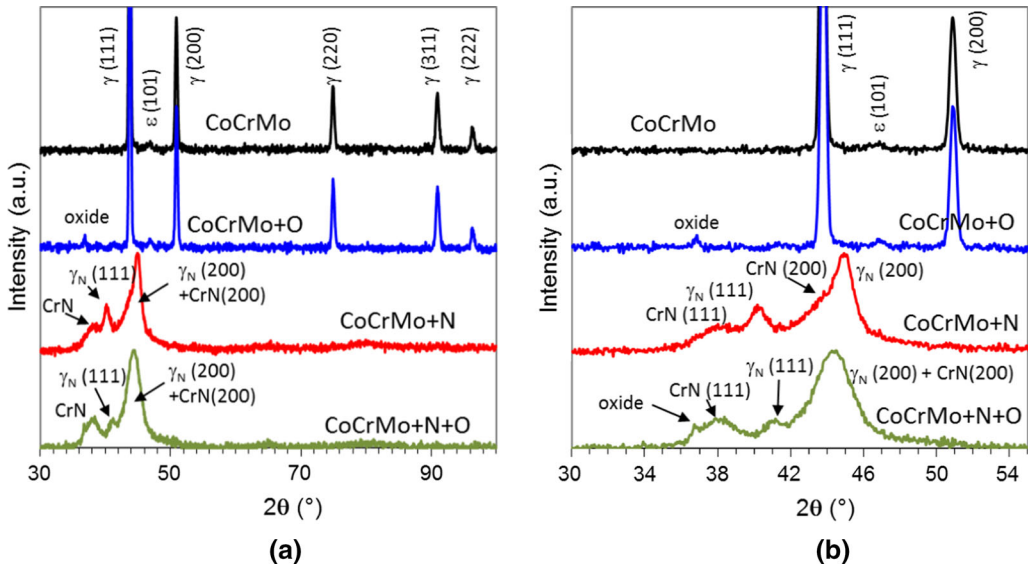

Fig. 2—Bragg-Brentano XRD patterns of (*a*) plasma-nitrided (red spectrum, CoCrMo + N), plasma-oxidized (blue spectrum, CoCrMo + O), and double-treated (green spectrum, CoCrMo + N + O) samples and (*b*) enlarged patterns. The XRD pattern of the untreated CoCrMo alloy is given in black as reference. While slight evolution is observed by XRD measurements after oxidation, the nitrided and the double-treated samples display characteristic peaks of an expanded γ_N phase (Color figure online).

0.9 pct NaCl at (37 ± 0.5 °C) in an AUTOLAB Potentio-Galvanostat (Eco Chemie, Netherlands) interfaced with a computer and recorder. A conventional three-electrode cell (EG&G PARR model) was used for all measurements. The cell was equipped with a saturated calomel reference electrode, a graphite auxiliary electrode, and a holder leaving only one side of the specimen exposed to the corroding medium. The electrolyte volume was systematically 800 mL. The sample surface always in contact with the testing solution was 1 cm^2. The open-circuit potential or corrosion potential E_{corr} was recorded after 30 minutes of stabilization, whereas rapid (50 V/hours) and slow scan rates (0.6 V/hours) were used. The investigation region was -1000 mV/E_{corr}/ + 1250 mV and each measurement was carried out twice to check the repeatability of the experiments.

D. *Metal Ions Released*

The concentration of the metal ions released in the solution was determined by Instrumental Neutron Activation Analysis (INAA) at the 2 MW pool-type research reactor (TU-Delft, The Netherlands). The samples were irradiated in high-purity polyethylene capsules together with a capsule filled with a certified reference material with a neutron dose 4.5 to 5.3 × 10^{16} neutrons×cm^{-2} s^{-1} (activation time 4 to 5 hours). The system uses a network of three gamma-ray spectrometers with well-type detectors and two gamma-ray spectrometers with coaxial detectors. The quality management system fulfills the requirements of the NEN-EN-ISO/IEC 17025:2005.[39]

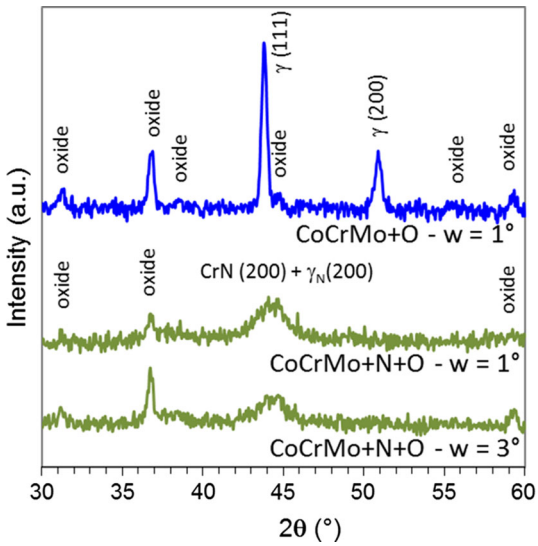

Fig. 3—GIXRD spectra of plasma oxidized (blue spectrum, CoCrMo + O) and double-treated (green spectrum, CoCrMo + N + O) CoCrMo samples. GIXRD was performed with incidence of 1 and 3 deg (Color figure online).

III. RESULTS

A. *Nitrided, Oxidized, and Double-Treated Samples*

1. *Elemental profiles*

The elemental profiles from GDOES measurements are presented in Figure 1 for the investigated samples. In this figure, the profiles on the left are expanded views of the overall profiles on the right and they represent the treated top surface layers (up to 0.4 μm). The overall profile for the nitrided CoCrMo alloy suggests a thick nitrided layer (max. N content ~ 26 at. pct) ranging over 5 μm in depth. In the case of the nitrided sample (Figure 1(a)), the formation of a thin surface oxy-nitrided layer can be observed, mainly consisting of Co, as can be seen in the expanded view of the overall profile (the Cr content is rather limited). The plasma oxidizing of the alloy leads to the formation of about 60-nm-thick surface layer mainly consisting of cobalt oxide (Figure 1(b)). No significant modification was observed underneath. The combination of nitriding followed by oxidizing (double treatment) results in a thicker (about 250 nm) oxidized layer, mainly consisting of cobalt oxide (the Cr presence is also limited within the first 100 nm–Figure 1(c)). The oxygen diffusion front is significantly broader compared to the plasma-oxidized CoCrMo alloy sample; no significant amount of oxygen was found in regions deeper than 300 nm. The nitrogen content of the nitrided layer below the oxide was a few percent lower than in the nitrided sample, indicating nitrogen diffusion to a deeper depth during the oxidizing treatment.

The elemental profiles obtained by RBS and NRA, presented elsewhere, reported higher values of nitrogen at the top surface layers.[35] However, they were in agreement with the GDOES results.

Averaged on a large surface area and over a depth of few hundreds nm, the EDS analysis gave a nitrogen content in the nitrided CoCrMo of about 30 at. pct. The EDS analysis of the oxidized and the double-treated samples is discussed in the next section according to the inhomogeneous microstructure of the treated layer.

2. *Phase analysis by X-ray diffraction*

XRD patterns obtained in the Bragg-Brentano geometry are shown in Figure 2 according to surface

Table I. Average Roughness Ra (nm) Measured by AFM on 30 × 30 μm at Different Regions

Sample	Region 1	Region 2	Region 3
CoCrMo	1.58	1.99	3.26
CoCrMo + N	45.3	41.3	41.7
CoCrMo + O	26.6	54.0	8.07
CoCrMo + N + O	40.8	50.7	58.1

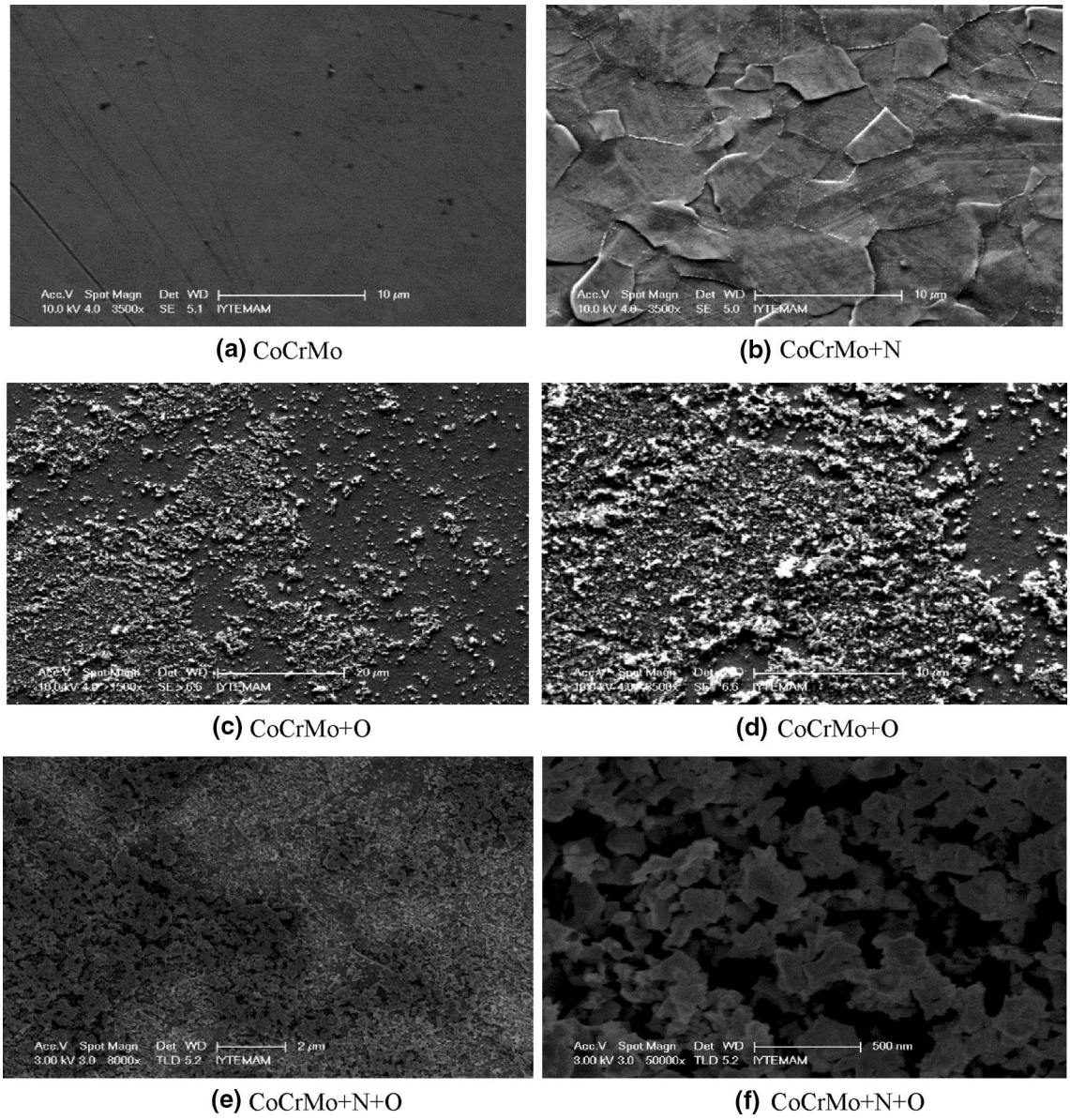

Fig.4—SEM images of (*a*) CoCrMo, (*b*) plasma-nitrided (CoCrMo + N), (*c*, *d*) plasma-oxidized (CoCrMo + O), and (*e*, *f*) double-treated (CoCrMo + N + O) CoCrMo samples.

treatments. The CoCrMo substrate alloy is characterized by the intense peaks of the main austenitic initial face-centered cubic (fcc) γ phase with a lattice constant of about 0.358 nm. A weak contribution is visible around 47 deg, attributed to the peak (101) of a small amount of hexagonal close packed (hcp) ε phase of CoCrMo.

As previously obtained with such treatment, the XRD data for the nitrided sample suggest the formation of an expanded phase, γ_N phase.[19,25] The initial γ and ε phases are no longer visible because the nitrided layer thickness is larger than the X-ray penetration depth. The expanded phase formation observed in this study is also similar to the ones formed in austenitic stainless steel alloys.[11] The expanded phase peaks, labeled as $\gamma_N(200)$ and $\gamma_N(111)$, were difficult to quantitatively analyze.[40] They are asymmetric, broad, and with different intensity ratios compared to the initial γ phase ones. These characteristics are relative to the crystallographic orientation-dependent diffusion in the various grains, leading to a nitrogen gradient through the X-rays probed depth, and to the high level of compressive stresses due to the expansion of the lattice by nitrogen insertion. Indeed, these stresses were shown in austenitic stainless steels to induce high density of defects by elastic and plastic responses (including grains rotation).[40,41]

Experimental XRD data in Figure 2 were fitted by a non-linear least squares curve-fitting routine to obtain accurate peak centers for the treated layer and substrate phases. The fitting function was Pearson VII. The average position of the γ_N-(111) and γ_N-(200) peaks corresponds to a lattice parameter of 0.388 and 0.405 nm, respectively. This difference in measured lattice expansion is usually associated with a different nitrogen

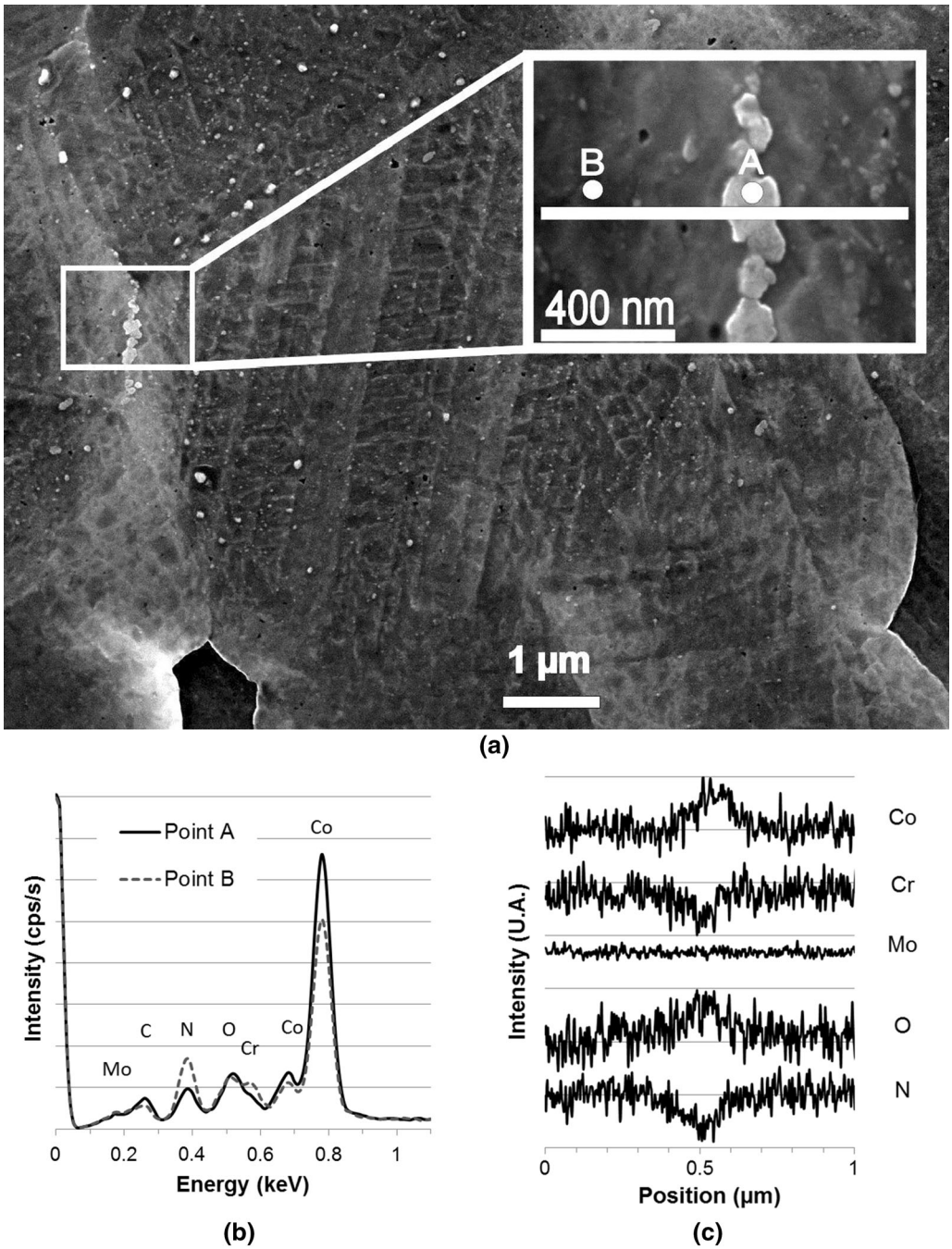

Fig. 5—(*a*) Secondary electrons SEM image of the surface of nitrided CoCrMo + N sample. The zoomed image indicates the position of the measurements (points A and B) of the EDS sprectra (*b*) and of the line scan of the EDS intensities through a surface particle (*c*).

content, a different stress field, and/or a different elasto-plastic behavior of the (200) oriented grains compared to the (111) ones. The XRD data for the plasma nitrided sample also show a broad peak around 2 theta ~ 37.7 deg, which is associated with the (111) peak of the cubic CrN phase (a = 0.413 nm). The CrN phase, which is likely formed as nanoparticles dispersed in the γ_N matrix may also contribute to the asymmetry of the wide peak in the range 42 to 45 deg as a result of its (200) contribution.

In addition to the peaks relative to initial γ and ε phases, the XRD data obtained on the oxidized CoCrMo sample show a small peak around 2θ ~ 36.8 deg. This peak suggests the formation of an oxide layer on the surface of the oxidized CoCrMo sample. To enhance the extreme surface layer contribution to the XRD signal, GIXRD were performed with incidence of 1 deg and 3 deg. The GIXRD data are presented in Figure 3 and from this figure oxide(s) peaks are more or less visible at 31.2, 36.8, 38.5, 44.8, 55.7, and

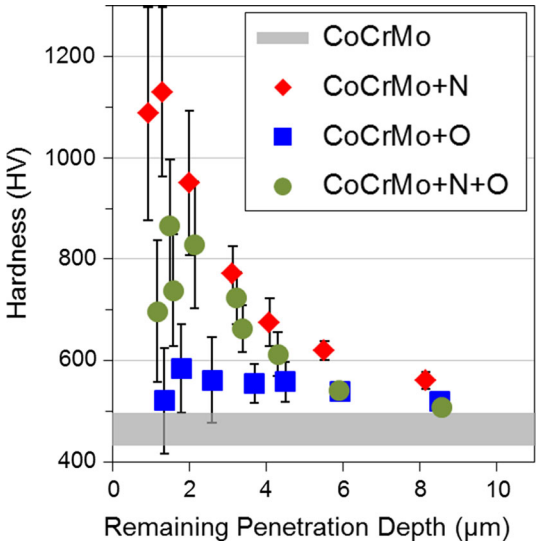

Fig. 6—Vickers microhardness as a function of the remaining indent or penetration depth (corresponding to increased loads from 25 to 500 g). Microhardness of bulk CoCrMo is about (465 ± 25) HV (gray range on the graph).

59.3 deg and can all be associated with the FCC cobalt oxide Co_3O_4 (JCPDS 42-1467). Peaks at 36.8, 55.7, and 59 deg might alternatively be attributed to the tetragonal CrO_2 phase (JCPDS 71-869).

In the case of the double-treated sample (CoCrMo + N + O sample), the intensity of the CrN peak at ~ 38 deg has increased compared to the nitrided CoCrMo sample (CoCrMo + N sample). Due to the redistribution of nitrogen in the metastable γ_N phase, a slight increase in the amount and/or particle size of the CrN phase is expected during the oxidation process (2 hours at 400 °C). The in-depth diffusion of nitrogen—as observed by GDOES—and the CrN formation-coarsening, both relative to the annealing, are expected to affect the expanded phase (γ_N) characteristics, reducing its nitrogen content and the compressive stress level. It means a lower intensity of the γ_N peaks and their shift towards the large angles. The observed peak at 41.1 deg can then be attributed to the shifted γ_N-(111) peak initially at 40.3 deg in the CoCrMo + N sample. On the other hand, the apparent shift of the peak around 44.4 deg toward the low angle side is likely due to an increase of the CrN-(200) contribution (~ 43.7 deg) to this asymmetric peak in conjunction with a lower γ_N-(200) peak intensity. Like in the CoCrMo + O sample, an oxide peak is visible at 36.7 deg in the $\theta/2\theta$ data and the same additional oxide peaks at 31.3 and 59 deg can be observed by GIXRD at 1 deg or 3 deg of incidence. It has to be said that the peak at 41.1 deg may also be associated with Cr_2O_3-(113) peak.

3. *Surface morphology investigation*

A visual inspection of the substrate and plasma-nitrided CoCrMo samples suggests macroscopically homogeneous surfaces. On the contrary, the oxidized (CoCrMo + O) and double-treated (CoCrMo + N + O) samples are non-homogeneously covered by purple-like dust particles (flakes), with weak adhesion.

Surface topography/structures of polished as well as treated CoCrMo samples were then investigated by atomic force microscopy. An average roughness (Ra) was estimated based on at least three measurements realized in three different areas (Table I). As usually observed with such plasma-assisted nitriding process, the nitrogen insertion in the γ phase induced the increase of the surface roughness because of the differential swelling of the various grains and of the plastic slip bands on some (all) grains (SEM Figures 4 and 5 in the following).[41] Within the observed area (30 μm × 30 μm), the roughness is then increased from 2 to 3 nm to about 42 nm.

Roughness values for the oxidized sample show a large variation, and this is attributed to the various regions on the surface of this sample. For example, the higher roughness value (~ 54 nm) is due to the high density of flake-like particles in region 2. On the other hand, the region 3 has a much smaller roughness (~ 8 nm) since there are no more flakes/particles in this region.

Even with the presence of particles, the CoCrMo + N + O sample shows little variation of the roughness from one region to another, likely because of the initial value of 42 nm of the nitrided substrate.

The SEM images of the substrate as well as nitrided, oxidized, and double-treated CoCrMo samples are shown in Figure 4. The CoCrMo substrate surface (Figure 4(a)) is characterized by some remaining polishing scratches. The SEM picture of the nitrided surface (Figure 4(b)) shows the elasto-plastic damages induced by the compressive stresses due to the nitrogen insertion and the lattice expansion. At the surface of one of the grains, slip bands with a specific orientation can be observed. The swelling is different from one grain to another, depending on the crystallographic orientation (anisotropic diffusion as well as anisotropic elasto-plastic response).[40–42] White spots are visible on the nitrided sample surface, especially at the grains or twins boundaries. The EDS line profile taken across a white particle localized at a grain boundary of the CoCrMo + N sample is shown in Figure 5. It is clearly evident that these particles are cobalt oxide and not chromium nitride.

Similar white snowflake-like structures, with size of less than few hundreds of nanometres, are observed in the case of the oxidized (Figures 4(c) and (d)) and double-treated surfaces (Figures 4(e) and (f)) but with much higher density. The distribution of these particles is much more uniform for the CoCrMo + N + O sample compared to the oxidized alloy and their size smaller. However, in both cases, there is no segregation at the grain boundaries as the sides of the entire grains can be covered.

For the oxidized CoCrMo alloy, three different regions were analyzed by EDS: (1) white particles themselves, (2) substrate region with no (or little) white particles, and (3) regions having combination of both 1 and 2. In region 1 (white particles), the oxygen content varied from 38 to 44 at. pct with about 40 at. pct of Co and only 12 at. pct of Cr. In region 2 (more like substrate), the oxygen content is about 17 at. pct with 26

at. pct of Cr, 3 at. pct of Mo, and 52 at. pct of Co: the initial metal ratio is here conserved. The region 3 exhibits intermediary compositions.

Similar EDS results were obtained on the CoCrMo + N + O sample: the white particles are rich in O (~ 50 at. pct) and Co (~ 40 at. pct), with only 7 at. pct of Cr and no detected nitrogen. A zone without white particles is presenting a composition in metallic elements close to the initial alloy, with ~ 18 at. pct of N and 16 at. pct of O.

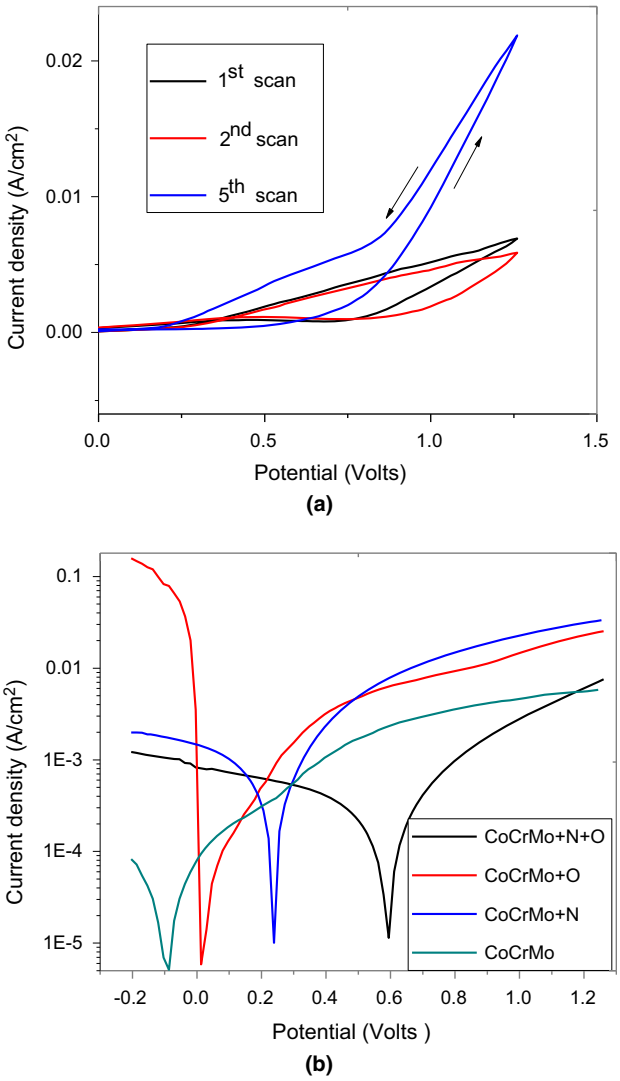

Fig. 7—Potentiodynamic polarization curves (*a*) for the nitrided sample (rapid scan rate) and (*b*) for the samples under investigation (slow scan rate).

4. *Microhardness*

Results of Vickers microhardness measurements are presented in Figure 6 as a function of the remaining indent depth. On each sample, several indentations were performed with different loads ranging from 25 to 500 g, leading to a remaining indent depth increasing from about 1 to 8 μm. Consequently, the microhardness value is not representative of the modified surface layer but includes a contribution of the layer underneath.

Compared to the substrate CoCrMo microhardness (465 ± 25) HV whatever the load, the oxidation treatment does not bring any significant modification, as expected from the very thin oxide layer detected by the other characterizations. After nitriding, the microhardness is improved up to (1100 ± 200) HV with the lowest loads, indicating a nitrided layer of few microns with hardness at least 3 times higher than that of the initial CoCrMo. The plasma oxidation of the nitrided layer (double treatment) seems to reduce the top surface microhardness to (800 ± 100) HV but there is no significant influence on the hardness measured with higher load compared to the nitrided sample.

B. *Corrosion Behavior of the Samples*

1. *Corrosion tests*

The substrate CoCrMo alloy and the modified surfaces were subjected to corrosion in 0.9 pct NaCl solution at body temperature (37 ± 0.5 °C). The samples were first allowed to stabilize under the open-circuit conditions until reaching a stable value of the corrosion potential. After that cyclic voltammetry (five rapid scans) and slow scan rate measurements were applied. Although these tests can be in most of the cases interpreted only qualitatively, significant information is obtained for the behavior of the metallic surface in a corrosive solution. The application of rapid scan rates leads to predictions of the corrosion behavior of the sample under constant conditions (without or with very thin coating formation), whereas the slow scan rates allow measurements under non-constant conditions of the metallic surface (coating formation) and the corroding medium providing information of the general corrosion.[37,38]

The value of the open-circuit potential E_{ocp} for the untreated alloy was – 220 mV while the corresponding values recorded for the modified samples shifted to the positive direction and were – 70, – 60, and – 50 mV for

Table II. Characteristics of the Slow Scan Corrosion Study (Values of Corrosion, Pitting, and Repassivation Potential, E_{cor}, E_{pit}, and E_{rep} and Current Density)

Sample	Treatment	E_{corr} (mV)	E_{pit} (mV)	E_{rep} (mV)	i_{max} (mA)
CoCrMo	reference	– 85	1430	1230	> 40
CoCrMo + N	nitriding	30	1430	1230	30
CoCrMo + O	oxidation	10	1030	1680	35
CoCrMo + N + O	nitriding + oxidation	595	1250	1750	21

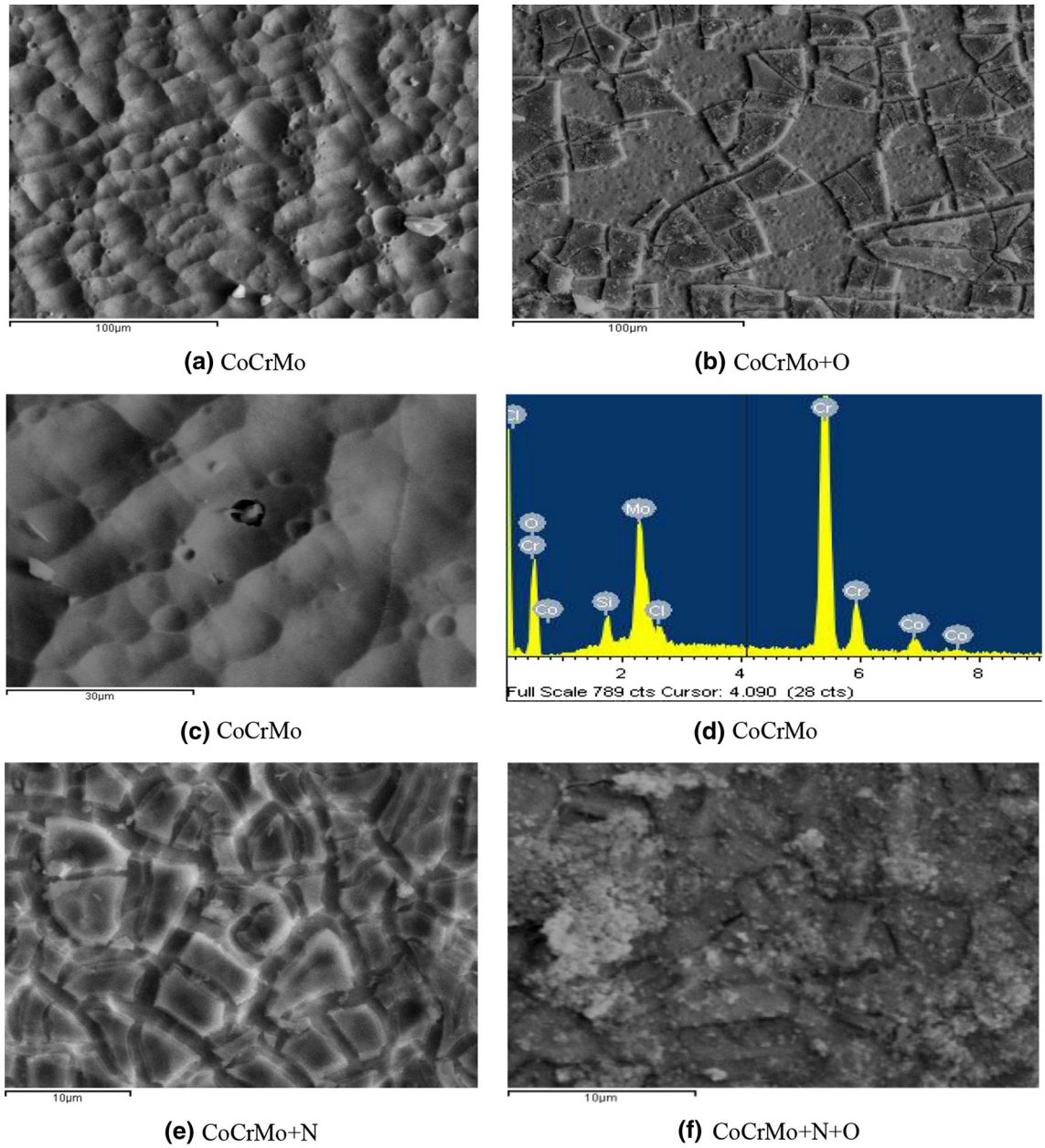

Fig. 8—SEM micrographs of the samples after corrosion: (*a*), (*c*) CoCrMo, (*b*) plasma-oxidized, (*e*) plasma-nitrided, (*f*) double-treated samples and (*d*) EDS analysis of CoCrMo.

the oxidized, nitrided, and double-treated sample, respectively. This indicates a reduction of the metal dissolution on the modified surfaces by affecting the anodic reaction. Different sweeps (rapid scan rate) of the nitrided sample are given in Figure 7(a). As it is shown, the shape of the subsequent sweeps remained the same during the initial scans and increased in the next demonstrating loss of the corrosion resistance.

The hysteresis loop observed during the reverse scan indicates sensitivity to localized corrosion. Similar behavior was observed for the oxidized sample and the untreated alloy with the i_{max} ranging from 5.5 up to 27 and 40 mA, respectively. The double-treated sample exhibited higher corrosion resistance with low current values (i_{max} 8.5 mA). The hysteresis loop was the same after subsequent scans during the cyclic voltammetry experiments showing the good quality of the protective film.

Representative potentiodynamic polarization curves obtained by slow scan rates are shown in Figure 7(b). These curves give information about the long-term corrosion behavior of the samples. The corresponding electrochemical parameters (values of the corrosion (E_{cor}), pitting (E_{pit}), repassivation potential (E_{rep}), and current (i_{max})) are given in Table II and explained in detail elsewhere.[43,44]

As can be seen from Figure 7(b) and the values of Table II, at lower potentials, the corrosion current is generally cathodic due to the reduction of water and

Table III. Average Roughness Ra (nm) Measured by AFM on 30 × 30 μm at Different Regions After Corrosion Tests

Sample	Region 1	Region 2	Region 3
CoCrMo	7.9	72	81
CoCrMo + O	22	21	122
CoCrMo + N	20	68	172
CoCrMo + N + O	22	76	77

dissolved oxygen. Then, the current passes through zero (at the E_{cor}) and remains low in the anodic region where a passivation plateau due to the formation of the passive oxide film is observed. Activation of the surface takes place at the E_{pit} and the current is rapidly increased reaching a maximum value (i_{max}). This is due to the spallation of the protective layer under application of high voltages. In the reverse scan, the current is decreased again, at the E_{rep}, because of the formation of a protective film leading to the repassivation of the surface. For the untreated alloy, it is obvious that the passivation region is narrow and the current values high. For the nitrided and oxidized samples, the values of the corrosion and pitting potential were nobler and the current values lower due to the enhanced thickness of the passive oxide. The repassivation potential was reduced indicating delay in the formation of the passive film in the reverse scan because of the higher surface roughness. In the case of the double-treated sample, the lower value of the i_{max} and the shift of the corrosion and repassivation potential to nobler direction indicated higher corrosion resistance.[37,38,43–45] The double-treated samples remained stable at the end of the corrosion tests.

The concentration of the metals in the solution after the electrochemical tests was significantly reduced after the treatment of the alloy surface. Especially in the case of the double treatment, the decrease of the metal ions released was 90 pct for the Co ions, 80 pct for the Mo ions, and 70 pct for the Cr ions, indicating the efficiency of the material for potential biomedical applications.

To sum up, the results of the polarization and cyclic voltammetry tests showed, for the modified samples, shift of the potential values to the positive direction and reduction of the current values, denoting an increase of the passive film thickness as it was verified by the characterization techniques (GDOES, RBS-NRA). The nitrided and oxidized samples exhibited almost similar behavior compared to the untreated alloy but with lower current densities and nobler E_{cor} values. On the other hand, higher variation of the potential and current values was observed in the case of the double-treated samples. One can conclude that while the plasma nitriding and plasma oxidation treatments slightly improve the corrosion resistance of the CoCrMo alloy, the treatment involving both leads to a significant improvement.

2. *Characterization of the samples after the corrosion tests*

The characterization of the corroded samples by RBS-NRA techniques revealed that in the case of the CoCrMo substrate, the corrosion proceeds in the near surface layers to a depth up to 750 nm. An extensive Co dissolution was observed in these layers. The thickness of the corroded layer was estimated to be 300 and 600 nm for the oxidized and the nitrided samples, respectively. The oxygen and especially the carbon peaks were found to increase in all samples after the corrosion.

In the case of the nitrided sample, the nitrogen profile showed that the nitrogen content was significantly decreased after the corrosion test, most probably due to dissolution. The sample with the double treatment was less corroded and the thickness of the modified layers remained practically unchanged: the nitrogen depth distribution was found to be the same with the non-corroded sample.[35]

The SEM-EDS and AFM analyses supported the corrosion data and the RBS-NRA findings. The SEM micrographs of the untreated alloy and the oxidized sample after the corrosion are shown in Figures 8(a) through (c). In the first case, the corrosive medium resulted in the formation of bubble-shaped grains at the surface with different constitution (Figures 8(a) and (c)). Following the EDS analysis on the untreated sample (Figure 8(d)), the concentrations of Co and Cr were 3 and 30 wt pct, respectively, in these grains. Different concentrations were detected in the bulk (48 and 25 wt pct, respectively) indicating that the corrosion preferentially occurred in specific sites by Co dissolution.[31,35] The oxidized sample exhibited a different depict with spallation of the protective oxide and areas with morphology similar to the ''uncoated'' surface (Figure 8(b)). In the corroded regions, Co concentration was low (~ 20 wt pct) and O concentration high (45 to 50 wt pct). Figure 8(e) shows the surface morphology of the nitrided specimen after corrosion. The corroded surface revealed that the crystals growth associated with the passivation. The Co (resp. Cr) concentration was varied from 8 to 30 (resp. 25 to 35 wt pct). However, a different morphology was presented by the double-treated specimen (Figure 8(f)). The surface seemed to be slightly affected by the corrosive solution and small size particles (nanocrystalline formations) aggregated to form larger size clusters leading also to higher surface roughness as was observed by the AFM investigation. The dissolution of Co and Cr was limited and the Co (resp. Cr) concentrations in different regions varied from 15 to 20 wt pct (resp. 27 to 47 wt pct).

Investigation by AFM at different regions (corroded and less affected by corrosion) gave similar results. From the AFM data, we obtained the average roughness (Ra) in nm. As can be seen in Table III, the average roughness was significantly increased after the corrosion and showed a large variation in several points. This

could be attributed to the corrosion process and the growth of new formations as was observed through the SEM-EDS investigation.

IV. DISCUSSION

A. *Effect of Nitriding, Oxidizing, and Double Treatment on CoCrMo Surface*

The sample characterization confirms that the plasma-assisted nitriding at 400°C leads to the formation of the usual FCC expanded phase γ_N and some precipitation of CrN nitrides. The nitrided layer exhibits improved mechanical properties. Few cobalt oxide particles can be observed at the surface, nearby the grain boundaries acting as nucleation sites; they likely come from oxidation by residual gas during the nitriding (or the heating under vacuum) and are favored by the poor reactivity of Co with nitrogen (enthalpy of formation of Co_3N: + 8.4 kJ/mol), whereas its relative high reactivity with oxygen (*e.g.*, enthalpy of formation of Co_3O_4: − 905 kJ/mol).[46]

After the plasma oxidation, XRD, RBS, and EDS analyses demonstrate the formation of a cobalt-rich oxide at the surface, whereas the formation of chromium oxide was limited. These cobalt oxides (possibly Co_3O_4 based on GIXRD but other oxides such as CoO or Co_2O_3 are not excluded) appear as non-protective and poorly adherent particles. In the GDOES profile of the CoCrMo + O sample, it is possible that a buried passivating Cr oxide was formed (around depth of 60 nm) but it is very thin and/or insufficiently crystallized to be formally detected by XRD or GDOES. The very sharp interface between the oxidized layer and the bulk CoCrMo suggests that such a passivating layer might prevent any deeper oxygen diffusion. All the observed modifications on the CoCrMo + O sample take place in a limited depth to induce detectable microhardness improvement.

Compared to the CoCrMo + O sample, the CoCrMo + N + O sample exhibits a deeper oxygen incorporation up to 300 nm and a broadened interface between the top Co-oxide layer (0 to 100 nm) and the underneath zone not modified by the oxidation (below 400 nm). Clearly, the previous nitriding of CoCrMo does not protect it from dry thermal oxidation. During the plasma oxidation of the CoCrMo + N sample, the thermal treatment destabilizes the metastable γ_N phase and promotes the coarsening of the CrN nitride particles in conjunction with slightly deeper nitrogen diffusion. With the induced Cr depletion in the remaining metal cell, less Cr is then available to create a thin passivating Cr oxide layer; on the contrary, the Co of the remaining γ_N phase is ready to be oxidized as it hardly reacts with nitrogen. All these factors could explain the observed increase of the oxygen penetration in the case of the CoCrMo + N + O sample in comparison to the CoCrMo + O sample. The high density of microstructural defects produced by the initial nitriding and the N and Cr re-organization is likely another reason for the higher oxygen penetration. Compared to the nitrided sample, the CoCrMo + N + O sample exhibits a slightly lower hardness, but only at the lowest loads (25 and 50 g, corresponding to remaining indent depths of 1.2 and 1.5 μm). Indeed, the nitrogen profile is not significantly modified until up to 5 μm and no hardness evolution at high loads is expected. On the contrary, the indentations at the lowest loads are more sensitive to the hardness evolution of the surface layer. The slight decrease of the hardness can be related to the poor mechanical resistance of the oxidized zone (ranging over 300 nm) and to the microstructure modifications induced in the nitrided zone by the annealing during the oxidation: coarsening of the CrN precipitates, destabilization of γ_N phase, and lower compressive stress.

B. *Influence of the Nitriding, Oxidizing, and Double Treatment on the Corrosion Resistance*

The investigation of the corrosion behavior reveals that the modified samples exhibited better corrosion performance suitable for biomedical applications especially after long exposure to the corrosive solution. This could be attributed to thick, hard, and resistant layers and the new surface microstructure produced by the plasma process.[31] As it is known, when the CoCrMo alloy is exposed to the solution, the surface is passivated under the formation of protective oxides. The most dominant constituent of the protective layer is the Cr_2O_3 due to the higher affinity of Cr to oxygen in comparison to Co and Mo and the corrosion proceeds mainly by Co dissolution.[6,30,31] The investigation of the corroded samples by RBS-NRA and SEM-EDS confirmed that the corrosion preferentially occurred by Co dissolution in specific sites and in modified regions of limited thickness.

The lowest corrosion resistance was exhibited by the oxidized CoCrMo alloy but still higher in comparison to the untreated alloy. This is because the formed passivating Cr_2O_3 oxide is too thin due to limited thickness of the modified surface layers. The samples subjected to nitriding displayed improved corrosion resistance due to the presence of nitrogen as well as the enhanced thickness of the modified layers.[30] The highest corrosion resistance was exhibited by the CoCrMo + N + O sample combining nitriding and oxidizing and the formation of a protective Cr_2O_3 oxide plus a thicker nitrogen-rich layer after the double treatment. As was revealed by RBS-NRA investigation of this sample, the nitrogen depth distribution was little affected by the corrosion treatment in comparison to the nitrided sample. It seems that the oxidation after the nitriding contributes to the formation of a stable nitrogen layer probably associated with the redistribution of nitrogen in the metastable γ_N phase, preventing the N-dissolution and resulting in the inhibition of the corrosion process. The beneficial role of the nitrogen on the corrosion resistance of the CoCrMo alloy or its composites after plasma nitriding or nitrogen implantation has been reported in the literature.[45,47,48] The samples in these studies exhibited the lowest deterioration after the corrosion tests and limited metal ions released, demonstrating their feasibility as biomedical implants.

V. CONCLUSIONS

To enhance the corrosion resistance, CoCrMo alloy was subjected to various surface treatments: plasma-assisted nitriding, plasma-assisted oxidizing, or a successive combination of both (double treatment). The nitriding led to the formation of a significantly hardened nitrided layer of a few micrometers, composed of an expanded γ_N phase with about 25 at. pct of nitrogen and some CrN precipitates. Without any modification of the surface microhardness in comparison to untreated CoCrMo, the oxidizing of CoCrMo was limited to about 60 nm and only a cobalt-rich oxide was detected as non-adherent surface layer. In the double treatment, the initial nitriding seemed to enhance the oxidation penetration: the oxygen profile was found to be broadened up to 300 nm but similar Co-rich oxides were detected at the surface. These observations could be attributed to the decomposition of the γ_N phase, leading to the coarsening of CrN precipitates, to the release of Co from the decomposed phase, and to the high-induced density of structural defects.

Nevertheless, the mechanical properties of the CoCrMo + N + O are kept similar to the properties of the nitrided sample. All the treatments led to an increase of the surface roughness and corrosion resistance and especially the double treatment. This is attributed to the combination of a thicker and more stable layer: oxidizing treatment led to formation of a thin protective oxide and nitriding was also effective to inhibit corrosion. The metal ions released were significantly reduced, especially in the case of the double treatment. In conclusion, oxidation plus nitriding considerably improves the mechanical properties of CoCrMo alloy and its corrosion resistance decreasing the metal ions released and these samples could be successfully used for biomedical applications.

ACKNOWLEDGMENTS

This work pertains to the French Government program ''Investissements d'Avenir'' (LABEX INTERACTIFS, Reference ANR-11-LABX-0017-01) and the IAEA–CRP 1576 ''Micro-analytical Techniques Based on Nuclear Spectrometry for Environmental Monitoring and Material Studies.'' The NAA measurements have been supported by the European Commission under the 7th Framework Programme through the 'Research Infrastructures' action of the 'Capacities' Programme, NMI3-II Grant Number 283883.''

REFERENCES

1. A.M. Ribeiro, T.H.S. Flores-Sahagun, and R.C. Parede: *J. Mater. Sci.*, 2016, vol. 51, pp. 2806–16.
2. N. Maruyama, H. Kawasaki, A. Yamamoto, S. Hiromoto, H. Imai, and T. Hanawa: *Mater. Trans.*, 2005, vol. 46, pp. 1588–92.
3. D. Bunea, D. Bojin, S. Zamfir, F. Miculescu, and M. Miculescu: *Eur. Cell Mater.*, 2003, vol. 5, pp. 53–54.
4. J. Lutz, C. Diaz, J.A. Garcia, C. Blawert, and S. Mändl: *Surf. Coat Technol.*, 2011, vol. 205, pp. 3043–49.
5. O. Öztürk, U. Türkan, and A.E. Eroglu: *Surf. Coat Technol.*, 2006, vol. 200, pp. 5687–97.
6. A. Bazzoni, S. Mischler, and N. Espallargas: *Tribol. Lett.*, 2012, vol. 49, pp. 157–67.
7. S. Virtanen, I. Milošev, E. Gomez-Barrena, R. Trebše, J. Salo, and Y.T. Konttinen: *Acta Biomater.*, 2008, vol. 4, pp. 468–76.
8. G. Bellefontaine: *The Corrosion of CoCrMo Alloys for Biomedical Applications*. Thesis of Master of Research, University of Birmingham, 2010.
9. J.M. Williams, L. Riester, R. Pandey, and A.W. Eberhardt: *Surf. Coat. Technol.*, 1997, vol. 88, pp. 132–38.
10. C. Díaz, J. Lutz, S. Mändl, J.A. García, R. Martínez, and R.J. Rodríguez: *Nucl. Instrum. Methods B*, 2009, vol. 267, pp. 1630–33.
11. H. Dong: *Int. Mater. Rev.*, 2010, vol. 55, pp. 65–98.
12. B.R. Lanning and R. Wei: *Surf. Coat. Technol.*, 2004, vol. 186, pp. 314–19.
13. A. Celik, A. Bayrak, A. Alsaran, A. Kaymaz, and A.F. Yetim: *Surf. Coat. Technol.*, 2008, vol. 202, pp. 2433–38.
14. J. Chen, X.Y. Li, T. Bell, and H. Dong: *Wear.*, 2008, vol. 264, pp. 157–65.
15. J. Lutz and S. Mändl: *Nucl. Instrum. Methods B.*, 2009, vol. 267, pp. 1522–25.
16. Q. Wang, C. Huang, and L. Zhang: *J. Mater. Sci. Technol.*, 2012, vol. 28, pp. 60–66.
17. B. Kaya, Ş. Yılmaz, and C. Ergun: *Defect Diffus Forum.*, 2010, vols. 297–301, pp. 82–87.
18. A. Çelik, M. Aslan, A.F. Yetim, and Ö. Bayrak: *J. Bion. Eng.*, 2014, vol. 11 (2), pp. 303–10.
19. L. Pichon, S. Okur, O. Ozturk, J.P. Riviere, and M. Drouet: *Surf. Coat. Technol.*, 2010, vol. 204, pp. 2913–18.
20. J. Lutz, J.W. Gerlach, and S. Mändl: *Phys. Status Solid. A.*, 2008, vol. 205, pp. 980–88.
21. J. Lutz and S. Mändl: *Surf. Coat. Technol.*, 2010, vol. 204, pp. 3040–46.
22. M.M.M. Bilek: *Appl. Surf. Sci.*, 2014, vol. 310, pp. 3–10.
23. Q. Wang, L. Zhang, and J. Dong: *J. Bion. Eng.*, 2010, vol. 7, pp. 337–44.
24. Q. Li, X.J. Zhou, Y.X. Leng, and N. Huang: *Gongneng. Cailiao. J. Funct. Mater.*, 2010, vol. 41, pp. 1324–30.
25. D.L. Williamson, O. Ozturk, R. Wei, and P.J. Wilbur: *Surf. Coat. Technol.*, 1994, vol. 65, pp. 15–23.
26. O. Öztürk, S. Okur, L. Pichon, M.O. Liedke, and J.P. Riviere: *Surf. Coat. Technol.*, 2011, vol. 205 (2), pp. 290–93.
27. J. Lutz and S. Mändl: *Plasma. Process. Polym.*, 2009, vol. 6, pp. 65–69.
28. Z. Werner, M. Barlak, M. Gradzka-Dahlke, R. Diduszko, W. Szymczyk, J. Dabrowski, J. Piekoszewski, and K. Borkowska: *Vacuum.*, 2007, vol. 81, pp. 1191–94.
29. J.A. Ortega-Saenz, M.A.L. Hernandez-Rodriguez, V. Ventura-Sobrevilla, R. Michalczewski, J. Smolik, and M. Szczerek: *Wear.*, 2011, vol. 271, pp. 2125–31.
30. Z. Guo, X. Pang, Y. Yan, K. Gao, A.A. Volinsky, and T.Y. Zhang: *Appl. Surf. Sci.*, 2015, vol. 347, pp. 23–34.
31. D.C. Ba, L. Xu, and Q. Wang: *Vacuum.*, 2015, vol. 119, pp. 214–22.
32. J.A. García, C. Díaz, S. Mändl, J. Lutz, R. Martínez, and R.J. Rodríguez: *Surf. Coat. Technol.*, 2010, vol. 204, pp. 2928–32.
33. *Ion Implant Technol*, ed., C. Diaz, and J.A. Garcia, and S. Maendl, and R. Pereiro, and B. Fernandez, and R.J. Rodriguez, and L. Pelaz, and I. Santos, and R. Duffy, and F. Torregrosa, and K. Bourdelle, eds., *Ion Implant Technol*, Am. Inst. Phys., Melville, 2012, pp. 284–87.
34. S. Mändl, C. Díaz, J.W. Gerlach, and J.A. García: *Nucl. Instrum. Methods B.*, 2013, vol. 307, pp. 305–09.

35. F. Noli, P. Misaelides, A. Lagoyannis, L. Pichon, and O. Ozturk: *Nucl. Instrum. Methods B.*, 2014, vol. 331, pp. 125 29.
36. L. Pichon, A. Straboni, T. Girardeau, M. Drouet, and P. Widmayer: *J. Appl. Phys.*, 2000, vol. 87, pp. 925–28.
37. *Corrosion Tests and Standards*, ed., R. Baboian, ed., *Corrosion Tests and Standards*, American Society for Testing and Materials, Philadelphia, 1995.
38. *Laboratory Corrosion Tests and Standards*, ed., A. Haynes, and R. Baboian, eds., *Laboratory Corrosion Tests and Standards*, American Society for Testing and Materials, Philadelphia, 1985.
39. P. Bode and M. Blaauw: *J. Radioanal. Nucl. Chem.*, 2012, vol. 291, pp. 299–305.
40. C. Templier, J. Stinville, P. Villechaise, P.O. Renault, G. Abrasonis, J.P. Riviere, A. Martinavicius, and M. Drouet: *Surf. Coat. Technol.*, 2010, vol. 204, pp. 2551–58.
41. J.C. Stinville, C. Templier, P. Villechaise, and L. Pichon: *J. Mater. Sci.*, 2011, vol. 46, pp. 5503–11.
42. R.M. Oliveira, C.B. Mello, G. Silva, J.A.N. Gonçalves, M. Ueda, and L. Pichon: *Surf. Coat. Technol.*, 2011, vol. 205, pp. 111–14.
43. F. Noli, P. Misaelides, A. Lagoyannis, and A. Akbari: *Nucl. Instrum. Methods B.*, 2011, vol. 269, pp. 3226–29.
44. J.P. Riviere, J. Delafond, P. Misaelides, and F. Noli: *Surf. Coat. Technol.*, 1998, vols. 100–101, pp. 243–46.
45. F. Noli, P. Misaelides, E. Pavlidou, and A. Lagoyannis: *Nucl. Instrum. Methods B.*, 2012, vol. 270, pp. 1–8.
46. *Smithells Metals Reference Book*, 7th Edition, E.A. Brandes, G.B. Brooks, 1998, pp. 8-24, 8-25.
47. Y.N. Petrov, G.I. Prokopenko, B.N. Mordyuk, M.I. Vasylyev, S.M. Voloshko, V.S. Skorodzievski, and V.S. Filatova: *Mater. Sci. Eng. C.*, 2016, vol. 58, pp. 1024–35.
48. K. Sadiq, R.A. Black, and M.M. Stack: *Wear.*, 2014, vol. 316, pp. 58–69.